Dehybridization of f and d states in the heavy-fermion system YbRh_{2}Si_{2}

D. Leuenberger, J. A. Sobota, S.-L. Yang, H. Pfau, D.-J. Kim, S.-K. Mo, Z. Fisk, P. S. Kirchmann, and Z.-X. Shen

Dehybridization of f- and d-States in the Heavy-Fermion System YbRh$_2$Si$_2$

D. Leuenberger,[1, 2] J. A. Sobota,[1, 2, 3] S.-L. Yang,[1, 2, *] H. Pfau,[1, 4] D.-J.
Kim,[5] S.-K. Mo,[3] Z. Fisk,[5] P. S. Kirchmann,[1, †] and Z.-X. Shen[1, 2, 4, ‡]

[1]*Stanford Institute for Materials and Energy Sciences,*
SLAC National Accelerator Laboratory, 2575 Sand Hill Road, Menlo Park, CA 94025, USA
[2]*Geballe Laboratory for Advanced Materials, Department of Applied Physics, Stanford University, Stanford, CA 94305, USA*
[3]*Advanced Light Source, Lawrence Berkeley National Laboratory, Berkeley, CA 94720, USA*
[4]*Department of Physics, Stanford University, Stanford, CA 94305, USA*
[5]*Department of Physics and Astronomy, University of California, Irvine, CA 92697, USA*
(Dated: February 26, 2018)

We report an optically induced reduction of the f-d hybridization in the prototypical heavy-fermion compound YbRh$_2$Si$_2$. We use femtosecond time- and angle-resolved photoemission spectroscopy to monitor changes of spectral weight and binding energies of the Yb $4f$ and Rh $4d$ states before the lattice temperature increases after pumping. Overall, the f-d hybridization decreases smoothly with increasing electronic temperature up to ~ 250 K but changes slope at ~ 100 K. This temperature scale coincides with the onset of coherent Kondo scattering and with thermally populating the first excited crystal electrical field level. Extending previous photoemission studies, we observe a persistent f-d hybridization up to at least ~ 250 K, which is far larger than the coherence temperature defined by transport but in agreement with the temperature dependence of the non-integer Yb valence. Our data underlines the distinction of probes accessing spin and charge degrees of freedom in strongly correlated systems characterized by spin-charge separation.

Strong electronic correlations in rare-earth intermetallic compounds lead to a series of remarkable properties such as the Kondo effect [1], heavy-fermion (HF) behavior [2], quantum criticality [3, 4], and unconventional superconductivity [5]. The Kondo effect is one of the quintessential observations involving strongly correlated electrons. The single-ion Kondo effect describes the spin-flip scattering of itinerant valence electrons on localized f-electron magnetic moments that leads to the formation of new composite quasiparticles. In a Kondo lattice f-electrons are periodically arranged and these composite quasiparticles form renormalized bands near the Fermi level (E_F) with extremely high effective masses [2, 6]. In turn, a renormalized so-called large Fermi surface develops as a result of the interaction between conduction electrons and f local moments. This spectral weight transfer to E_F is accompanied by an intermediate valence configuration with a non-integer f-occupation [7, 8]. A complimentary spectroscopic signature of the Kondo lattice effect is the hybridization band gap Δ between the renormalized f-band and the valence electron band [9–11]. Despite much work, the strong electronic correlations in Kondo lattice systems pose serious challenges for theoretical calculations. In particular, it is still debated how the Kondo lattice effect emerges and how the electronic band structure evolves as the temperature is lowered [8, 12, 13].

YbRh$_2$Si$_2$ (YRS) is considered a prototypical Kondo lattice system in which itinerant Rh $4d$ electrons scatter on a lattice of localized Yb $4f$ moments. The lowest lying $J = 7/2$ multiplet of the Yb $4f$ states is split by the crystal electric field (CEF) into four Kramers doublets [14]. Different experimental probes distinguish several cross-

over temperature scales in YRS: The single-ion Kondo temperature $T_K \approx 25$ K is defined as the characteristic spin fluctuation temperature and is experimentally determined by neutron scattering, specific heat measurements and an extremum in the thermopower [15–17]. The Kondo effect is related to spin-flip scattering, which becomes coherent in Kondo lattices, resulting in a maximum of the resistivity at $T_{coh} \approx 100$ K [16]. This resistivity maximum can be influenced by the CEF splitting [18] and departs from the conventional expectation that $T_{coh} < T_K$ [19].

While thermodynamic and transport properties in Kondo system are dominated by spin degrees of freedom, angle-resolved photoelectron spectroscopy (ARPES) is sensitive to charge degrees of freedom. Accordingly, ARPES observes a renormalized f-band close to E_F, a hybridization gap in the electronic band structure [10, 11, 20], and a large Fermi surface [21, 22]. Tunneling spectroscopy correlates the hybridization gap to spectral signatures which disappear above 25 K [12]. However, temperature dependent ARPES shows no change of the large Fermi surface and the expected transition to a small Fermi surface was not observed up to 100 K [8]. Conventional ARPES studies at even higher temperatures are challenging due to thermal broadening [8].

Here, we study the hybridization and spectral weight of d- and f-states in YRS with femtosecond time-resolved ARPES (trARPES) [23, 24]. Optical excitation of electron-hole pairs raises the electronic temperature while the lattice remains largely unperturbed preventing spectral broadening at short time scales. We analyze the spectral weight and binding energy changes and observe a continuous decrease of f-d hybridization as function of

electronic temperature. The hybridization gap remains finite up to the highest measured electronic temperature of 250 K. This temperature dependence is consistent with the change of Yb valence but is disconnected from the smaller T_K and T_{coh} temperature scales. We explain this difference by the sensitivity of transport and thermodynamics measurements to spin degrees of freedom while photoemisssion accesses charge degrees of freedom. Additionally, the temperature dependence of the f spectral weight suddenly changes slope at 100 K, which coincides with two comparable temperature scales: populating the first excited CEF level and T_{coh}. This kink is distinct from the smooth temperature dependence of the hybridization gap and the Yb valence and thus points to physics beyond a mean field description.

Our trARPES setup [25] is based on an amplified Ti:Sa laser system operating at 312 kHz repetition rate. Samples are optically excited with 35 fs pump pulses at $h\nu = 1.5$ eV photon energy. Electrons are photoemitted as function of pump-probe delay with probe pulses at $4h\nu = 6$ eV and collected in a hemispherical electron analyzer as sketched in Fig. 1(a). The total energy resolution is 22 meV; the time resolution is 160 fs. Single crystals of YRS have been grown in the body-centered tetragonal structure using the high temperature Indium flux method as described in reference [17]. Samples are cleaved *in situ* and oriented parallel to the crystallographic *a-b* plane. The pressure was $< 1 \times 10^{-10}$ Torr and the base temperature was 20 K for all measurements.

Fig. 1 shows trARPES spectra recorded near the $\overline{\Gamma}$-point at 1 ps before (a) and during optical excitation (b). We observe three electronic bands below E_F, labeled (1), (2) and (3). According to high resolution ARPES measurements [8, 10, 11, 21, 26, 27] and DFT slab calculations [21, 24, 27], bands (1) and (2) are assigned to hole-like Rh $4d_{xy}$ and Rh $4d_{xz/yz}$ bands, respectively. Band (3) corresponds to the renormalized Yb $4f$ level. Our 22 meV energy resolution and the low cross section for $4f$-states at a photon energy of 6 eV [24, 28] prevents us from resolving the CEF splitting of the $4f^{13}$ states. Optically excited electrons populate bands (4) and (5), which originate from Rh $4d$ orbitals according to slab calculations [24, 27].

To understand how hybridization mixes orbital characters and changes band dispersions it is instructive to consider the periodic Anderson model (PAM) [2, 29]. A simplified version was successfully applied to equilibrium ARPES results on YRS [10, 11] and other heavy fermion compounds [13, 30–32]. In a mean-field hybridization approach to the PAM the dispersion relations

$$E^{\pm}(k) = \frac{\epsilon_d(k) + \epsilon_f}{2} \pm \sqrt{\left(\frac{\epsilon_d(k) - \epsilon_f}{2}\right)^2 + \Delta^2} \quad (1)$$

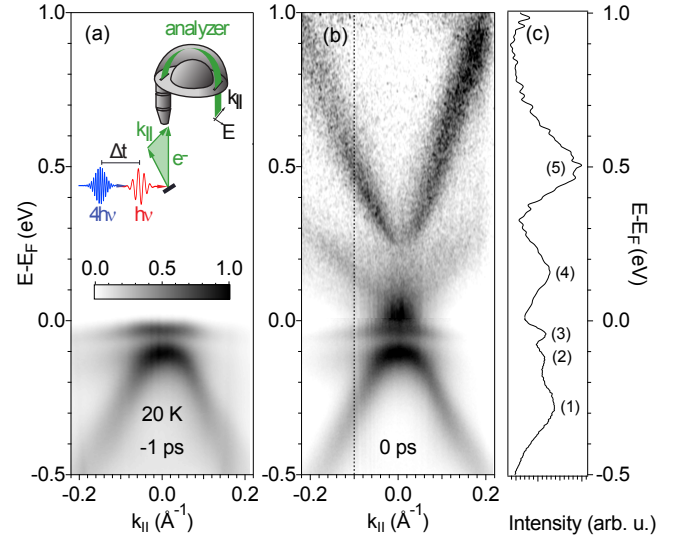describe the hybridized Rh $4d$ and Yb $4f$ band in the Kondo lattice state. A hybridization gap Δ separates

FIG. 1: Band structure of YRS at 20 K measured with trARPES at 6 eV photon energy near the $\overline{\Gamma}$-point, (a) 1 ps before and (b) during the presence of a 0.5 mJ/cm^2 infrared pump pulse. (c) EDC taken at $k_{\parallel} = -0.1$ Å^{-1}. In addition to the bands (1)-(3) below E_F, bands (4) and (5) are transiently populated by optically excited electrons. Intensities are rescaled exponentially as a function of energy for enhanced visibility of the transient features above E_F. Inset in (a) sketches the trARPES geometry.

the renormalized Yb $4f$ band from the Rh $4d_{xy}$ and Rh $4d_{xz/yz}$ bands. $\epsilon_d(k)$ and ϵ_f refer to their dispersions before hybridization. We approximate $\epsilon_d(k)$ by a quadratically dispersing band and ϵ_f by a momentum independent band. Δ is the mean-field hybridization gap which we assume to be momentum independent.

We begin by assessing the equilibrium situation before optical excitation. $E^{\pm}(k)$ are plotted in Fig. 2(d) using $\Delta = 40$ meV, $\epsilon_f = -55$ meV, $\epsilon_d(k = 0) = -85$ meV and an effective mass of $-0.85\,m_e$. Our choice of values is consistent with previous ARPES results [8, 11, 21] as long as the CEF splitting, which we cannot resolve, is neglected. E^+ matches the observed dispersion of band (3) in Fig. 2(a). Hybridization leads to admixture of $4d$-character into the $4f$ band and introduces dispersion to the $4f$ band around $\overline{\Gamma}$. $E^-(k)$ matches band (2) in Fig. 2(a) and admixture of $4f$ states decreases the photoionization cross section for low photon energies [24, 28].

We compare the band structure 1 ps before and 0.2 ps after optical excitation in Fig. 2(a). The corresponding energy distribution curves (EDCs) are shown in Fig. 2(b). Fig. 2(c) is a difference plot of ARPES intensity before and after pumping based on the data in Fig. 2(a). We highlight two observations: First, the photoemission yield increases within the hybridization region and close to $\overline{\Gamma}$ (region II), and band (2) shifts towards E_F. Second, the photoemission yield of band (3) decreases as seen in
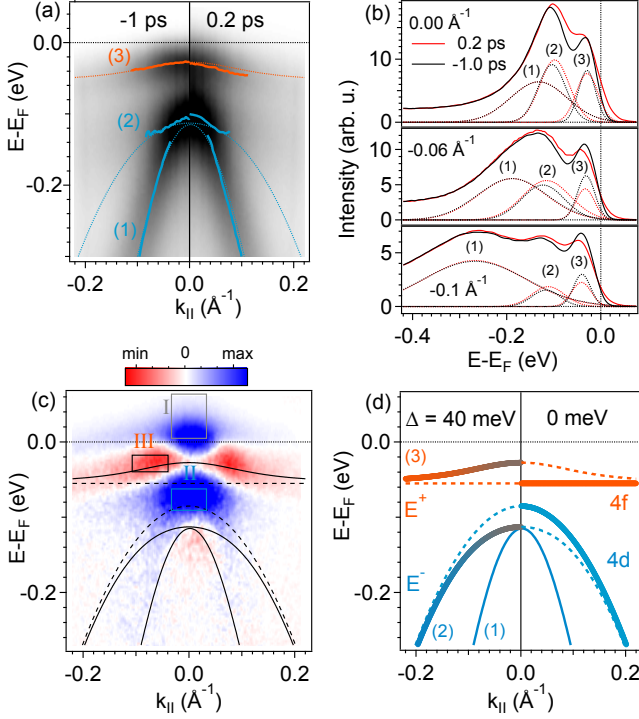
FIG. 2: (a) Band structure of YRS measured 1 ps before and 0.2 ps after optical excitation with 0.5 mJ/cm². The solid lines are the dispersions derived from EDC fits and the dotted lines show $E^{\pm}$. (b) Solid lines are EDCs taken from (a) at three different momenta. Dashed lines are fits to the EDCs. Bands (1), (2) and (3) are indicated. (c) shows the difference between the spectra. Region I integrates the photoelectron yield above E_F; region II integrates the spectral weight within the hybridization region; region III integrates the intensity of the hybridized $4f$-band. (d) The band dispersion $E^{\pm}(k)$ from Eq. 1 is plotted for $\Delta = 40$ meV and $\Delta = 0$ meV. Shading represent the calculated admixture of d-(f-)character to $E^+ (E^-)$.

the EDCs in Fig. 2(b) and in region III in Fig. 2(c). This effect is most pronounced close to the $\overline{\Gamma}$-point and diminishes for larger momenta.

We explain the pump-induced changes of the photoemission yield by dehybridization within the mean-field approximation: Optical excitation of electron-hole pairs around E_F reduces the gap Δ, which in turn renormalizes $E^{\pm}(k)$ according to Eq. 1: First, the effective mass of band (2) decreases and the band apex shifts towards E_F. This shift and the the decreasing f-admixture to the d band increases the photoemission yield in region II. Second, band (3) regains f character and hence loses intensity in region III. The observed momentum dependence qualitatively follows the calculated admixture of d character to the f states as shown in Fig. 2(d). We conclude that the pump-induced spectral changes qualitatively mimic those induced by raising the equilibrium temperature.

To quantitatively analyze how optical excitation affects the band structure, we introduce the concept of a transient electronic temperature T_e and distinguish electronic and lattice heating effects. In thermal equilibrium, electrons and lattice are at the same temperature. This is markedly different after ultrafast optical excitation, which solely couples to the electronic subsystem and initially leaves the lattice temperature unchanged. Electron-phonon coupling transfers energy from excited electrons to the lattice at later times, typically on a ps time scale. This behavior is commonly approximated in the 2-Temperature Model, which treats electrons and lattice as two coupled heat baths with distinct electronic and lattice temperature [33]. trARPES directly accesses T_e by measuring the width of the Fermi Dirac (FD) distribution at E_F. In practice, we determine an effective temperature T_{eff} by fitting a FD distribution to the EDCs. The finite energy resolution of our system of $\Delta E = 22$ meV is accounted for by extracting $T_e = [T_{eff}^2 - (\Delta E / 4k_B)^2]^{1/2}$ [34].

Notably, the line shapes of the EDCs in Fig. 2(b) remain unchanged upon optical pumping for energies outside of the hybridization region. In contrast, the linewidth doubles in temperature-dependent ARPES between 12 to 110 K [20]. We attribute this distinction to different lattice temperatures: ultrafast spectral changes of hybridization features are related to changes of T_e while the lattice temperature remains unaffected. Conversely, the overall broadening of the spectra in temperature dependent ARPES is induced by increasing lattice temperature. Thus, trARPES allows us to single out electronically driven spectral changes without blurring the spectra due to elevated lattice temperatures, provided that the band structure is probed at small enough delays after excitation.

We proceed to study the delay dependence of the ultrafast dynamics to identify the time scale on which effects of an elevated T_e dominate. Fig. 3(a) shows the dynamics after pumping with an incident fluence of 0.6 mJ/cm² in a difference plot of photoemission spectra with respect to equilibrium conditions at 20 K recorded at $k_{\parallel} = 0.06 \, Å^{-1}$. The broadening of the FD after pumping leads to an increase (decrease) of photoemission intensity above (below) E_F and is also visible in the EDCs in Fig. 2(b). The photoemission intensity at $E - E_F \approx -0.1$ eV increases after pumping as band (2) gains d-character which increases the photoemission cross section.

We analyze the dynamics in the spectral regions I-III and of T_e in detail in Fig. 3(b). The overall time resolution of our experiment of 160 fs is given by the width of the cross correlation (XC) at $E - E_F = 0.3$ eV. Region I tracks the intensity increase above E_F and is expected to be proportional to T_e for a thermalized electron distribution [35]. Indeed, both quantities track each other closely and peak at 0.2 ps before decaying on a ps time scale.
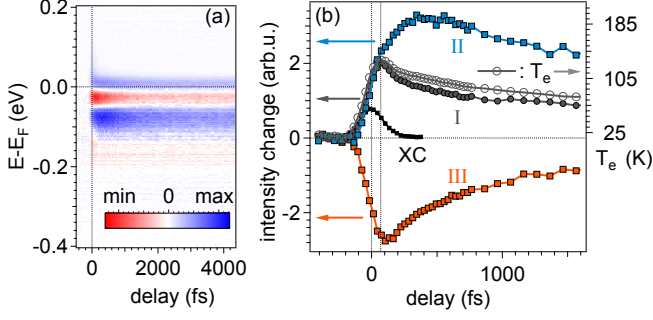
FIG. 3: (a) Changes in the photoemission spectra with respect to equilibrium conditions at $20\,\mathrm{K}$ as function of pump-probe delay, recorded at $k_\parallel = 0.06\,\mathring{A}^{-1}$ along $\overline{\Gamma}\text{-}\overline{X}$ at an incident fluence of $0.6\,\mathrm{mJ/cm^2}$. (b) Traces I-III correspond to the integrated photoelectron yields as function of pump-probe delay from the corresponding areas in Fig. 2(c). The transient T_e values are extracted by FD fits. The photoelectron intensity $0.3\,\mathrm{eV}$ above E_F yields the cross correlation (XC).

We attribute the ps relaxation dynamics after $0.2\,\mathrm{ps}$ to cooling of the electron distribution as electron-phonon coupling transfers energy to the lattice subsystem, and subsequent heat transport.

The decrease in region III tracks the decreasing admixture of $4d$ states. The increase in region II is related to the shift of band (2) toward E_F due to the reduced hybridization, and the increased photoemission yield due to decreasing $4f$ character. Recording these observables simultaneously allows us to correlate the dehybridization dynamics as monitored in regions II and III with T_e and the intensity in region I. The minimum of the intensity in region III coincides with the maximum of T_e and the maximum of intensity in region I. The spectral weight in region II initially also follows the rise of T_e. After $0.2\,\mathrm{ps}$ the increase slows down and the intensity peaks at $\sim 0.5\,\mathrm{ps}$. The fast rise tracks the optically induced dehybridization, while the later rise until $0.5\,\mathrm{ps}$ can be explained by spectral broadening of bands (1) and (2) due to the delayed rise of the lattice temperature [36]. This demonstrates that the optically induced ultrafast dehybridization is driven by the initial fast increase of T_e within $0.2\,\mathrm{ps}$.

Consequently, we can study the dehybridization without significantly changing lattice degrees of freedom by controlling T_e as the optical excitation density is varied. The spectra in Fig. 4(a) are recorded at a delay of $0.2\,\mathrm{ps}$, after which a thermalized FD distribution with a well defined T_e is established, but before elevated lattice temperatures broaden spectral features. The excitation density ranges from 0.2 to $1.4\,\mathrm{mJ/cm^2}$ which corresponds to $T_e = 56 - 249\,\mathrm{K}$ at a fixed delay of $0.2\,\mathrm{ps}$.

Fig. 4(b) shows that the intensity in region I above E_F increases linearly with increasing T_e, confirming the expected linear relationship for a thermalized electron
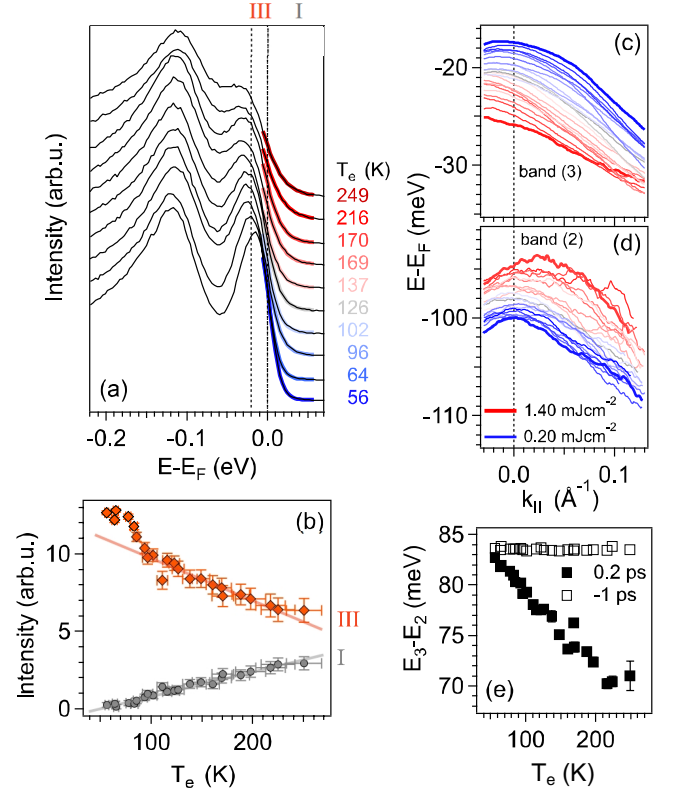

FIG. 4: (a) EDCs at $k_\parallel = 0.06\,\mathring{A}^{-1}$, measured at $0.2\,\mathrm{ps}$ as function of optical excitation density which is mapped onto T_e by fitting FD distributions. (b) Spectral weight of band (3) integrated in region III and region I above E_F plotted as function of T_e. (c) and (d) show the dispersion of bands (2) and (3), respectively, determined from EDC fits as function of excitation density at $0.2\,\mathrm{ps}$. (e) The energy difference of the maxima of bands (2) and (3) is extracted from the dispersions in (c) and (d) $1\,\mathrm{ps}$ before and $0.2\,\mathrm{ps}$ after optical excitation and plotted as function of T_e at $0.2\,\mathrm{ps}$.

population [35]. In the discussion of Fig. 2 and Fig. 3 we identified that direct spectral signatures of dehybridization are observed in region III. Accordingly, the photoemission yield in region III decreases smoothly with increasing T_e as the f admixture to the d states decreases. However, at $T_e \sim 100\,\mathrm{K}$ the slope changes visibly.

In addition to the spectral intensities, we analyze the dispersions of the $4f$ band and the $4d$ band as function of excitation density in Fig. 4(c) and (d) at a constant delay of $0.2\,\mathrm{ps}$. The energy difference $E_3 - E_2$ of the maxima of bands (2) and (3) is plotted in Fig. 4(e). For negative delays, before arrival of the pump pulse, $E_3 - E_2$ remains constant as function of excitation density, evidencing that pump-induced sample heating before time zero is avoided. At a fixed delay of $0.2\,\mathrm{ps}$, $E_3 - E_2$ decreases linearly with increasing T_e.

In Fig. 4, the intensity in region III and the band separation $E_3 - E_2$ continue to decrease linearly up to the

highest measured $T_e \approx 250\,\text{K}$. For a fully dehybridized band structure, we expect the intensity in region III and the energy difference $E_3 - E_2 \approx 30$ meV to be constant as function of temperature. Therefore, we conclude that YRS shows spectral signatures of hybridization up to $250\,\text{K}$. Our observation agrees with the persistence of the large Fermi surface up to $100\,\text{K}$ in equilibrium ARPES [8]. We corroborate our conclusion by considering that the renormalized f spectral weight at E_F is directly connected to an intermediate Yb valence [7]. In the temperature range of our measurement, the Yb valence increases smoothly from 2.96 to 2.98 [8] but remains non-integer. This confirms that f spectral weight at E_F is present and can hybridize with the d-band. Likewise, ARPES studies of the heavy fermion compound $CeCoIn_5$ detect signatures of hybridization up to the highest measured temperature of $200\,\text{K}$ [13]. Our findings are in contrast to tunneling spectroscopy, which observes signatures of the hybridization gap only below $25\,\text{K}$ [12].

	T_K	T_{coh}	T_{CEF}	T_{kink}
$YbRh_2Si_2$	$25\,\text{K}$	$100\,\text{K}$	$200\,\text{K}$	$100\,\text{K}$
	[15–17]	[16]	[11, 14]	this work
$CeCoIn_5$	$2\,\text{K}$	$40\,\text{K}$	$100\,\text{K}$	$50\,\text{K}$
	[37]	[37, 38]	[39]	[13]

TABLE I: Characteristic temperature scales in $YbRh_2Si_2$ and $CeCoIn_5$

We can speculate that the hybridization gap vanishes at temperatures as high as $600\,\text{K}$ when we assume a linear temperature dependence of Δ and extrapolate eqn (1) to a vanishing gap. Similarly, the Yb valence only assumes an integer value of 3 at an extrapolated value of more than $1000\,\text{K}$ [8]. Likewise, the temperature below which a large Fermi surface forms in $CeCoIn_5$ was estimated to be $270\,\text{K}$ [13]. The temperature scale of $600\,\text{K}$ in YRS can only serve as a rough estimate as it is obtained within a mean-field PAM without including CEF levels. At such high temperatures, excited CEF levels are populated and contribute to incoherent Kondo scattering.

The slope of the temperature dependent intensity in region III changes at $T_e = 100\,\text{K}$, while $E_3 - E_2$ evolves linearly as function of temperature. The f spectral weight and hybridization gap are connected smoothly in the mean-field PAM. Thus, the deviation from the linear, smooth temperature dependence of both quantities indicates that physics beyond the mean-field PAM is required to describe the Kondo lattice state. Our observations are similar to the change of slope of the f spectral weight around $50\,\text{K}$ in $CeCoIn_5$ [13]. In both compounds, the kink temperature T_{kink} coincides with two comparable temperatures scales (Table I): the coherence temperature T_{coh} and the temperature at which the first excited CEF level, which is separated from the ground state by $k_B T_{CEF}$, starts to be populated. On one hand,

the thermal population of the first excited CEF level can be assumed to be a smooth function of temperature and is unlikely to lead to a sudden change in the f spectral weight. On the other hand, a change of the Kondo scattering from incoherent to coherent affects the spectral line shape which can abruptly change the f spectral weight in a fixed energy range.

In summary, we monitor ultrafast light-induced changes of spectral weight and binding energies in the heavy Fermion compound $YbRh_2Si_2$ and provide evidence for dehybridization of localized f- and itinerant d-states. We extend the (electronic) temperature range of previous ARPES studies to $250\,\text{K}$ by recording spectral changes $0.2\,\text{ps}$ after optical excitation. In this non-equilibrium state, the lattice remains cold and only the electronic subsystem increases in temperature. We find that the hybridization of $4f$ and $4d$ states persists up to at least $T_e = 250\,\text{K}$, which is considerably higher than T_{coh}. The formation of the large Fermi surface and of the hybridization gap are therefore not coupled to the onset of coherence as accessed by experimental probes sensitive to spin degrees of freedom. However, our observation is consistent with the temperature dependence of the non-integer Yb valence and highlights the sensitivity of ARPES to charge degrees of freedom. We identify an intermediate temperature scale of $T_{kink} = 100\,\text{K}$ at which the spectral intensity of the hybridized $4f$ band changes discontinuously. This fine structure could be connected to the onset of coherence and hints towards physics beyond a mean-field PAM. Our work introduces a novel time domain approach for studying the emergence of heavy quasi particles in a Kondo lattice system without the influence of increased lattice temperatures. Future studies can extend the electronic temperature range further and may observe a full dehybridization and study its functional form to aid theoretical descriptions beyond mean field theory.

* Present address: Kavli Institute at Cornell for Nanoscale Science; Laboratory of Atomic and Solid State Physics, Department of Physics; Department of Materials Science and Engineering. Cornell University, Ithaca, New York 14853, USA

† Electronic address: `kirchman@stanford.edu`

‡ Electronic address: `zxshen@stanford.edu`

[1] J. Kondo, Prog. Theor. Phys. **32**, 37 (1964).

[2] A. C. Hewson, *The Kondo Problem to Heavy Fermions* (Cambridge University Press, Cambridge, England, 1993).

[3] H. v. Löhneysen, A. Rosch, M. Vojta, and P. Wölfle, Rev. Mod. Phys. **79**, 1015 (2007).

[4] P. Gegenwart, Q. Si, and F. Steglich, Nat. Phys. **4**, 186 (2008).

[5] C. Pfleiderer, Rev. Mod. Phys. **81**, 1551 (2009).

[6] P. Coleman, AIP Conf. Proc. **629**, 79 (2002).

[7] K. Kummer, Y. Kucherenko, S. Danzenbächer, C. Krellner, C. Geibel, M. G. Holder, L. V. Bekenov, T. Muro, Y. Kato, T. Kinoshita, et al., Phys. Rev. B **84**, 245114 (2011).

[8] K. Kummer, S. Patil, A. Chikina, M. Güttler, M. Höppner, A. Generalov, S. Danzenbächer, S. Seiro, A. Hannaske, C. Krellner, et al., Phys. Rev. X **5**, 011028 (2015).

[9] L. Degiorgi, Rev. Mod. Phys. **71**, 687 (1999).

[10] S. Danzenbächer, Y. Kucherenko, D. V. Vyalikh, M. Holder, C. Laubschat, A. N. Yaresko, C. Krellner, Z. Hossain, C. Geibel, X. J. Zhou, et al., Phys. Rev. B **75**, 045109 (2007).

[11] D. V. Vyalikh, S. Danzenbächer, Y. Kucherenko, K. Kummer, C. Krellner, C. Geibel, M. G. Holder, T. K. Kim, C. Laubschat, M. Shi, et al., Phys. Rev. Lett. **105**, 237601 (2010).

[12] S. Ernst, S. Kirchner, C. Krellner, C. Geibel, G. Zwicknagl, F. Steglich, and S. Wirth, Nature **474**, 362 (2011).

[13] Q. Y. Chen, D. F. Xu, X. H. Niu, J. Jiang, R. Peng, H. C. Xu, C. H. P. Wen, Z. F. Ding, K. Huang, L. Shu, et al., Phys. Rev. B **96**, 045107 (2017).

[14] O. Stockert, M. Koza, J. Ferstl, A. Murani, C. Geibel, and F. Steglich, Physica B **378380**, 157 (2006), proceedings of the International Conference on Strongly Correlated Electron Systems SCES 2005.

[15] O. Stockert, M. Koza, J. Ferstl, C. Geibel, and F. Steglich, Science and Technology of Advanced Materials **8**, 371 (2007), chemical Physics of Solids.

[16] O. Trovarelli, C. Geibel, S. Mederle, C. Langhammer, F. M. Grosche, P. Gegenwart, M. Lang, G. Sparn, and F. Steglich, Phys. Rev. Lett. **85**, 626 (2000).

[17] U. Köhler, N. Oeschler, F. Steglich, S. Maquilon, and Z. Fisk, Phys. Rev. B **77**, 104412 (2008).

[18] Y. Lassailly, A. K. Bhattacharjee, and B. Coqblin, Phys. Rev. B **31**, 7424 (1985).

[19] G. Zwicknagl, Physica Scripta **1993**, 34 (1993).

[20] S.-K. Mo, W. S. Lee, F. Schmitt, Y. L. Chen, D. H. Lu, C. Capan, D. J. Kim, Z. Fisk, C.-Q. Zhang, Z. Hussain, et al., Phys. Rev. B **85**, 241103 (2012).

[21] S. Danzenbächer, D. V. Vyalikh, K. Kummer, C. Krellner, M. Holder, M. Höppner, Y. Kucherenko, C. Geibel, M. Shi, L. Patthey, et al., Phys. Rev. Lett. **107**, 267601 (2011).

[22] M. Güttler, K. Kummer, S. Patil, M. Höppner, A. Hannaske, S. Danzenbächer, M. Shi, M. Radovic, E. Rienks, C. Laubschat, et al., Phys. Rev. B **90**, 195138 (2014).

[23] U. Bovensiepen and P. S. Kirchmann, Laser & Photonics Reviews **6**, 589 (2012).

[24] K. Kummer, D. V. Vyalikh, L. Rettig, R. Cortés, Y. Kucherenko, C. Krellner, C. Geibel, U. Bovensiepen, M. Wolf, and S. L. Molodtsov, Phys. Rev. B **86**, 085139 (2012).

[25] S.-L. Yang, J. A. Sobota, D. Leuenberger, Y. He, M. Hashimoto, D. H. Lu, H. Eisaki, P. S. Kirchmann, and Z.-X. Shen, Phys. Rev. Lett. **114**, 247001 (2015).

[26] G. A. Wigger, F. Baumberger, Z.-X. Shen, Z. P. Yin, W. E. Pickett, S. Maquilon, and Z. Fisk, Phys. Rev. B **76**, 035106 (2007).

[27] D. V. Vyalikh, S. Danzenbächer, Y. Kucherenko, C. Krellner, C. Geibel, C. Laubschat, M. Shi, L. Patthey, R. Follath, and S. L. Molodtsov, Phys. Rev. Lett. **103**, 137601 (2009).

[28] J. J. Yeh and I. Lindau, At. Data Nuc. Data Tables **32**, 1 (1985).

[29] P. W. Anderson, Phys. Rev. **124**, 41 (1961).

[30] S. Danzenbächer, Y. Kucherenko, M. Heber, D. V. Vyalikh, S. L. Molodtsov, V. D. P. Servedio, and C. Laubschat, Phys. Rev. B **72**, 033104 (2005).

[31] S. Danzenbächer, Y. Kucherenko, C. Laubschat, D. V. Vyalikh, Z. Hossain, C. Geibel, X. J. Zhou, W. L. Yang, N. Mannella, Z. Hussain, et al., Phys. Rev. Lett. **96**, 106402 (2006).

[32] H. J. Im, T. Ito, H.-D. Kim, S. Kimura, K. E. Lee, J. B. Hong, Y. S. Kwon, A. Yasui, and H. Yamagami, Phys. Rev. Lett. **100**, 176402 (2008).

[33] P. B. Allen, Phys. Rev. Lett. **59**, 1460 (1987).

[34] T. J. Kreutz, T. Greber, P. Aebi, and J. Osterwalder, Phys. Rev. B **58**, 1300 (1998).

[35] C. L. Smallwood, T. L. Miller, W. Zhang, R. A. Kaindl, and A. Lanzara, Phys. Rev. B **93**, 235107 (2016).

[36] J. Demsar, R. D. Averitt, K. H. Ahn, M. J. Graf, S. A. Trugman, V. V. Kabanov, J. L. Sarrao, and A. J. Taylor, Phys. Rev. Lett. **91**, 027401 (2003).

[37] S. Nakatsuji, S. Yeo, L. Balicas, Z. Fisk, P. Schlottmann, P. G. Pagliuso, N. O. Moreno, J. L. Sarrao, and J. D. Thompson, Phys. Rev. Lett. **89**, 106402 (2002).

[38] C. Petrovic, P. G. Pagliuso, M. F. Hundley, R. Movshovich, J. L. Sarrao, J. D. Thompson, Z. Fisk, and P. Monthoux, J. Phys.: Condens. Matter **13**, L337 (2001).

[39] E. D. Bauer, A. D. Christianson, J. M. Lawrence, E. A. Goremychkin, N. O. Moreno, N. J. Curro, F. R. Trouw, J. L. Sarrao, J. D. Thompson, R. J. McQueeney, et al., Journal of Applied Physics **95**, 7201 (2004).